Abstract—**The lateral superior olive is the first neural area to receive binaural inputs in the mammalian sound localization pathway. Selective to interaural level differences (ILD) while intensity-independent, these neurons signal when a sound arrives from within a limited range of angles. Although several different computational models have been proposed to explain**

A second class of models have used the fact that higher input intensities produce input signals with shorter latency, allowing one signal to arrive before the other [5],[6]. These models *are* biologically-justified, although most examples emphasize the timing aspect and use intensity-independent inputs with solely additive effects to determine firing. In this type of model, variable synaptic weighting can provide the different ILD-thresholds in the population.

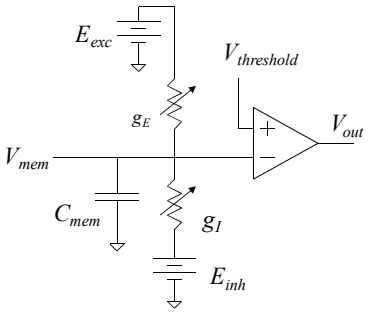

Fig. 2. Excitatory and inhibitory conductances determine the steady-state membrane potential which is a function of the ratio of excitation to inhibition.

A third class of LSO model (which does not preclude using the intensity-latency tradeoff effect mentioned above) emphasizes intensity-dependent excitatory and inhibitory synaptic conductances that compete to drive the membrane potential above a fixed threshold voltage [7], [8]. Unlike the models (like those discussed earlier) that treat excitation as *addition* and inhibition as *subtraction*, true biological synaptic input is best described as a conductance between the membrane potential and a fixed potential that determines whether it activates or suppresses neural activity. In these models, the "voltage-divider" (created by the excitatory and inhibitory conductances) determines the response (see Fig 2).

If $g_E = S_E \cdot \alpha \cdot h_L(\theta)$ and $g_I = S_I \cdot \alpha \cdot h_R(\theta)$, (2a,b)

and the definition $ILD = 20 \cdot \log\left(\frac{h_R(\theta)}{h_L(\theta)}\right)$, (3)

it can be shown that

$$V_{mem} = \frac{S_I \cdot 10^{\frac{ILD}{20}}}{S_E + S_I \cdot 10^{\frac{ILD}{20}}} E_{inh} + \frac{S_E}{S_E + S_I \cdot 10^{\frac{ILD}{20}}} E_{exc} \quad (4)$$

V_{mem} asymptotically charges towards a weighted sum of the excitatory reversal potential (E_{exc}) and the inhibitory reversal potential (E_{inh}) and is independent of the intensity α. A fixed threshold voltage can be used for all neurons and the ILD threshold is set by S_E and S_I.

A feature of this model is that the membrane capacitance is not used as a mathematical integrator which would be sensitive to initial conditions; the capacitor contributes instead to the low-pass filter characteristic of the neuron, where residual charge remaining from a previous computation (e.g., an earlier echo) affects only the latency of the response.

More than a specific model for sound intensity comparison, this is a general mechanism for neural computations that require ratio calculations.

II. Circuit Model

The conductance neuron circuit (Fig. 3) was based on the subthreshold current-mode approach by Arthur and Boahen [9] where the membrane potential is represented as a current and where the excitatory and inhibitory synaptic conductances are controlled by input currents. In this circuit, qualitatively, *Ii* pulls *Vx* up to *Vdd* with constant current and *Ie* pulls *Vx* down towards Vb with a rapidly diminishing current as *Vx* drops. *Vx* is transformed by M9 into a current (I_{Vmem}) that represents the membrane potential in (Fig. 2). A spiking mechanism resets the neuron once the I_{Vmem} exceeds the threshold current defined by V_{thresh}.

With *Vb* set about 0.7V below *Vdd*, M2 will operate as a triode-region pFET when Vx < Vb and as a pn-diode (source-well diode) in parallel with a pFET when Vx > Vb. Using the pFET subthreshold equation ($V_{well} = Vs$):

$I_D = I_0 e^{\frac{\kappa Vsg}{V_T}} \left(1 - e^{\frac{Vsd}{V_T}}\right)$, *Ie* pulls V_{syn_e} to $Vb - \frac{V_T}{\kappa} \ln \frac{Ie}{I_0}$.

The three important steady-state cases are:

(1) When *Ie* = 0, *Ii* pulls *Vx* towards *Vdd* against the M2 well-diode. The minimum I_{Vmem} is zero current.

(2) When *Ii* = 0, $I_{M4} = I_{M5} = Ie/2$, M2 operates in triode and *Vx* sits less than 0.1V below *Vb*. I_{Vmem} is near its maximum.

(3) When *Ie* = *Ii*, *Vx* = *Vb*.

There are three regions of operation for transistor M2:

(I) $Vb - 0.1V < V_x < Vb$ (M2 triode),

(II) $Vb < V_x < Vb + 0.1V$ (M2 triode || well-diode), and

(III) $Vb + 0.1V < V_x$ (M2 saturation || well-diode).

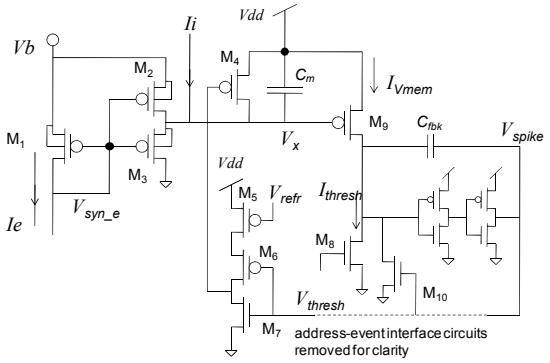

Fig 3. Neuron circuit with excitatory (*Ie*) and inhibitory (*Ii*) inputs that control the synaptic "conductance". The current I_{Vmem} represents the membrane potential V_{mem} in Fig. 2, which is compared to a current threshold I_{thresh}. C_m=270fF and C_{fbk}=30fF. The neuron output is a short digital voltage spike on the node V_{spike}. Transistors M1, M2, M3, and M9 (W/L in microns) are all 1.8/1.8 and M8 is 1.8/1.2.

Immediately following a neuron reset (M4 turned on transiently with a digital pulse) Vx will be close to Vdd (region I) and will decrease as the well-diode, M2, and M3 all draw current to pull it down. If Ii > Ie, then Vx will remain in either region I or II. If Ie > Ii, then we will enter region III. Because we are most interested in cases where excitation exceeds inhibition (although not exclusively), we consider the equations of region III in more detail. Assuming

all pFET I_0 terms to be the same,

$$Ii + I_0 e^{\frac{\kappa(Vb-V_{syn\_e})}{V_T}}\left(1-e^{\frac{-(Vb-Vx)}{V_T}}\right) - I_0 e^{\frac{\kappa(Vx-V_{syn\_e})}{V_T}} = C\frac{dVx}{dt} \quad (5)$$

If $I_{Vmem} = I_0 e^{\frac{\kappa(Vdd-Vx)}{V_T}}$ and $Ie = I_0 e^{\frac{\kappa(Vb-V_{syn\_e})}{V_T}}$ (6) (7)

We can differentiate equation (6) and plug in (5) and (7) to obtain (through simplification):

$$\frac{dI_{Vmem}}{dt} = \frac{-\kappa}{CV_T}\left[(Ii+Ie)I_{Vmem} - Ie\left(I_{Vmem}^{\frac{\kappa-1}{\kappa}}\left(I_0 e^{\frac{\kappa(Vdd-Vb)}{V_T}}\right)^{\frac{1}{\kappa}} + I_0 e^{\frac{\kappa(Vdd-Vb)}{V_T}}\right)\right] \quad (8)$$

Except for the $Ie \cdot I_{Vmem}$ product term, this equation appears to be a first-order linear system with a time-constant $\tau \approx CV_T / \kappa(Ii+Ie)$. It can be shown that the third term is much larger than the second term when $Vb > Vx$. Since region III is defined by $Vb > Vx$, the trajectory of I_{Vmem} appears like a first-order linear system through most of region III. Although region III only has a tiny dynamic range (< 100mV), this is sufficient to produce a 50-fold change in output current. By selecting a threshold current near the top of this range, we can ensure that most of the dynamic range of I_{Vmem} occurs in region III.

Although we cannot solve for the steady-state I_{Vmem} analytically here, we can see (by dividing both sides by Ii) I_{Vmem} can be expressed a function of the ratio Ie/Ii and should not be sensitive to simultaneous scaling of Ie and Ii:

$$0 = \frac{-\kappa}{CV_T}\left[\left(1+\frac{Ie}{Ii}\right)I_{Vmem} - \frac{Ie}{Ii}\cdot I_0^{\frac{1}{\kappa}}\cdot I_{Vmem}^{\frac{\kappa-1}{\kappa}}\cdot e^{\frac{Vdd-Vb}{V_T}} - \frac{Ie}{Ii}\cdot I_0 \cdot e^{\frac{\kappa(Vdd-Vb)}{V_T}}\right] \quad (9)$$

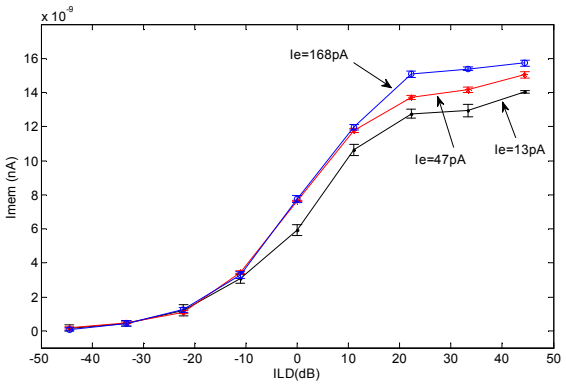

Fig. 4. Steady-state I_{Vmem} vs. "ILD". A copy of I_{Vmem} was measured using a simple current-sense amplifier off-chip. Holding Ie fixed, Ii was sampled at different current ratios (ILDs). The plot shows that the steady-state "membrane potential" (represented as a current) varies with the ILD, but weakly with the level of the input currents. This produces an acceptable level of intensity-independence desired for sound localization.

III. Circuit Testing

This circuit was fabricated in a commercially-available 3-metal, 2-poly, 0.5µm CMOS process.

A. Response to ILD at the Membrane Potential

In the first phase of testing, constant current inputs were provided as I_e and I_i, to demonstrate the steady-state performance of the conductance circuit. In the experiment shown in Fig. 4, the steady-state values of I_{Vmem} are shown for five different I_e / I_i ratios ("ILD"). The three curves represent different I_e and I_i levels. As expected from equations (8) and (9), scaling I_e and I_i does not change the steady-state I_{Vmem}, but does change the rate of charging. To obtain neurons with different ILD thresholds, different gain combinations for Ie and Ii are chosen to represent different "synaptic" S_E and S_I in equations 2a and 2b).

B. ILD-Selective Firing Patterns

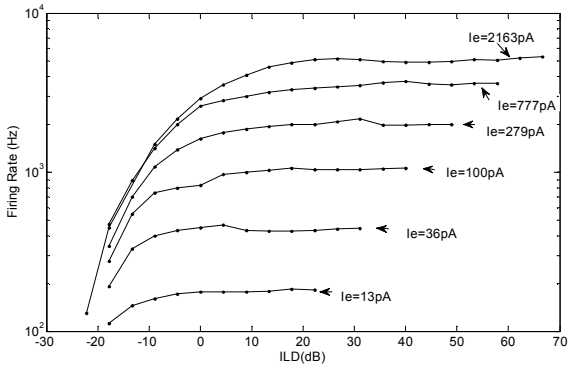

Fig. 5. Firing Frequency vs. input current ratio (ILD). This plot shows that the ILD of complete inhibition is nearly constant (~ -20dB) across different intensities (i.e., Ie and Ii are scaled together). Points shown are for ILDs that produced spiking output. Input currents are DC levels.

By selecting the excitatory and inhibitory input gains, a particular ILD selectivity emerges. Fig. 5 shows a series of plots where the excitation was held fixed and the inhibition was swept across a range of values to determine the ILD at which the neuron begins to fire. As expected from equation (9), (and Fig 4) the neuron begins to fire spikes within a very narrow range of ILD. As expected from equation (8), higher overall intensities produce higher firing rates.

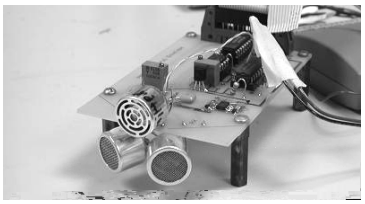

Fig. 6. Photo of the binaural sonar used in testing the LSO neuron chip. The inputs to the chip during the loud, outgoing echolocation pulse were strongly attenuated to simulate the middle-ear muscle attenuation in mammalian ears that attenuates self-generated sounds.

IV. Echolocation System Testing

To demonstrate the utility of the neural model of LSO for processing sonar signals, a narrowband (~ 40kHz) sonar system using short pulses (0.5 ms duration) was used to generate envelope signals of echoes (Fig. 6). The envelope of the returning echoes were extracted and converted approximately linearly to the currents I_e and I_i in real-time via

an analog interface circuit (not shown).

These demonstrations are significantly different from the earlier sections in three important ways: transient input signals, background noise, and multiple echoes.

A. Single-Target ILD-Selectivity and Range-Independence

Using different combinations of gain on the left and right microphone signals, multiple ILD-threshold settings are obtainable (Fig. 7).

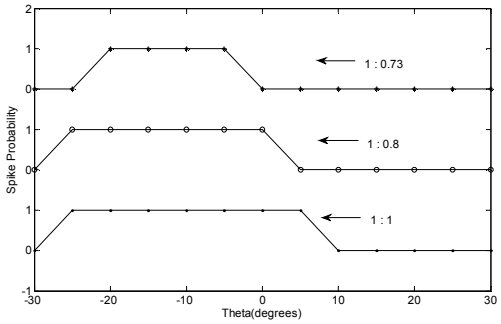

Fig. 7. Plot of spiking probability for three different synaptic gain combinations (top, middle, and bottom plots) to obtain different ILD thresholds. The inhibition to excitation ratio is shown for each graph. A target was presented at a fixed range of 16 inches. The response drops at large negative angles because targets at those angles no longer produce a significant echo due to the specific geometry of our sonar system.

To demonstrate intensity-independent ILD selectivity, we varied the range of the target object (4" dia. cardboard tube) and measured the ILD selectivity. In this experiment, the physical range over which the ILD selectivity remained relatively constant was rather limited. Although intensity-independence was demonstrated with DC currents (see section II), weak echoes (i.e., inputs) require a longer time for I_{Vmem} to reach steady-state. As a result, the short echolocation pulses did not provide the inputs for long enough to produce spikes at longer ranges where the signal was weaker. This can be solved by using a smaller capacitance for C_m.

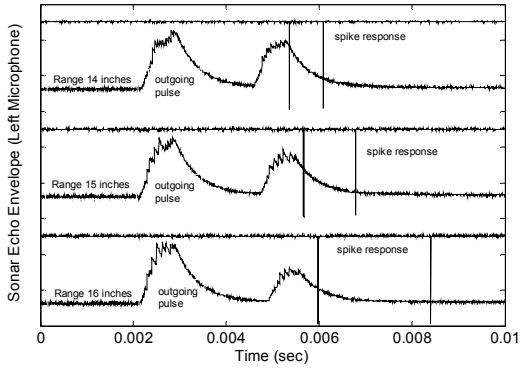

Fig. 8. Echo intensity affects response latency. When short duration stimuli are used, a valid ILD sound may not produce a spike due to the long latency of the response. The input signals are suppressed during the outgoing sound.

Interestingly, this argues for biological LSO neurons (which would suffer from the same problem) to have very short integration windows (~ 1ms) during echoes or a time-dependent gain mechanism. Additionally, equation (9) shows that if both inputs were compressed by a power-law (but not logarithmically), the working range of intensity-independent ILD-thresholding could be extended.

B. Latency vs. Amplitude: Limitations of Short Sounds

To graphically emphasize the effect of short stimuli, Fig. 8 shows the effect of echo amplitude on the latency of response. In the cases shown, the object direction is close to the threshold direction (ILD), meaning that the steady-state I_{Vmem} is close to the neuron's threshold. For three slightly different ranges (14 inches, 15 inches, and 16 inches) without changing the direction, the echo intensity drops sufficiently to produce a significant delay in the first spike. If the echo sound is short, the driving stimulus disappears before the spike can occur and the estimated ILD is incorrect.

C. Multiple Target Response

The response of the neuron to multiple targets was also tested to demonstrate that the neuron would not change its ILD selectivity when a preceding echo left the neuron with an arbitrary initial charge. ILD selectivity for a target at a range of 16 inches was measured first alone and then again with a preceding target (range = 10 inches, direction = 10 degrees). The ILD selectivity was unchanged (data not shown), indicating that the first echo (although it had suppressed the membrane potential only ~ 900μs earlier) did not change the response (i.e., spatial tuning) to the second echo.

ACKNOWLEDGMENT

The authors thank the MOSIS Educational Program for the continued support for chip fabrication of student projects.

REFERENCES

[1] Covey, E. and Casseday, J. H., "The Lower Brainstem Auditory Pathways" in *Hearing by Bats*, eds. Popper, A. N. and Fay, R. R., Springer-Verlag, NY. ISBN: 0-387-97844-5, 1995.

[2] Reed, M. C., and Blum, J. J., "A model for the computation and encoding of azimuthal information by the lateral superior olive", J. Acoust Soc Am, 88(3), pp. 1442-1453., 1990.

[3] Horiuchi, T. and Hynna, K. M. "Spike-based Modeling of the ILD System in the Echolocating Bat", Neural Networks, vol. 14, pp. 755-762, 2001.

[4] Shi, R. Z. and Horiuchi, T. K., "A Neuromorphic VLSI Model of Bat Interaural Level Difference Processing for Azimuthal Echolocation", IEEE Trans. Circuits and Systems I, vol. 54(1), pp. 74-88, 2007.

[5] Shi, R., and Horiuchi, T., "A VLSI model of the bat lateral superior olive for azimuthal echolocation", Proceedings of the 2004 International Symposium on Circuits and Systems (ISCAS'04), May 23- 26, 2004.

[6] Fontaine, B. and Peremans, H., "Tuning bat LSO neurons to interaural intensity differences through spike-timing dependent plasticity", Biological Cybernetics, 97(4), pp. 261-267., 2007

[7] M. Zacksenhouse, D. H. Johnson, J. Williams, and C. Tsuchitani, "Single-neuron modeling of LSO unit responses," J. Neurophysiol., vol. 79, pp. 3098–3110, 1998.

[8] Diranieh, Y. M., "Computer-Based Neural Models of Single Lateral Superior Olivary Neurons", M. S. Thesis, Boston University, Boston, MA. 1992.

[9] Arthur, J. V. and Boahen, K., "Silicon Neurons that Inhibit to Synchronize", Proc. Intl Symp Circ and Sys, May 24-26, 2006. Pp. 4807-4810. 2006.